

# Reservoir Description using a Binary Level Set Model

Lars Kristian Nielsen\*, Xue-Cheng Tai†, Sigurd Ivar Aanonsen‡ and Magne Espedal§

## Abstract

We consider the inverse problem of permeability estimation for two-phase porous media flow. In the parameter estimation process we utilise both data from the wells (production data) and spatially distributed data (from time-lapse seismic data).

The problem is solved by approximating the permeability field by a piecewise constant function, where we allow the discontinuity curves to have arbitrary shape with some forced regularity. To achieve this, we have utilised level set functions to represent the permeability field and applied an additional total variation regularisation. The optimisation problem is solved by a variational augmented Lagrangian approach.

The level set method of choice is a binary level set formulation which has the ability to both determine the curves of discontinuities and the constant values for each region. We do not need any initial guess for the geometries of the discontinuities, only a reasonable guess of the constant levels is required.

**Keywords:** Inverse problems, reservoir description, parameter identification, two phase flow, level set methods, augmented Lagrangian optimisation, total variation regularisation.

## 1 Introduction

Predictions of the reservoir behaviour require estimates of the reservoir property values, such as permeability and porosity, on a grid block scale. Even if all available data sources are utilised this can be a very difficult task. Large scale permeability trends, like barriers and channels, have large impact on how the fluids flow in the porous medium. Information of these structures is therefore important for the reservoir engineers controlling the production in the reservoir.

Available data types for estimating permeability and porosity inside a reservoir are geological data, seismic data and static and dynamic well data. The geological data are usually coarsened geological permeability maps, and the seismic data are several seismic surveys taken at different times through the production history. The seismic data contains information of fluid movement and pressure changes. The static well data can be obtained from core samples in the wells, while the dynamic well data are time series of pressures and flow rates in the wells.

Neither the seismic data nor the dynamic well data give any direct information of the permeability and porosity fields. Using the equations of fluid flow we can though use the indirect information from these measurements to estimate the permeability and the porosity on a coarse scale. A problem of this kind is generally known as an inverse problem, or more specific referred to as a *history matching* problem. In this paper we focus on the problem of recovering the permeability trends by utilising the information from the wells (both static and dynamic) together with the seismic data.

Because of the high costs of drilling a well, the well data is available from only a very small part of the reservoir, but the time frequency of this data can be high. Contrary to the well data, the

---

\*Department of Mathematics, University of Bergen and CIPR-Centre for Integrated Petroleum Research, University of Bergen (larskn@mi.uib.no)

†Department of Mathematics, University of Bergen and CIPR-Centre for Integrated Petroleum Research, University of Bergen (tai@mi.uib.no)

‡CIPR-Centre for Integrated Petroleum Research, University of Bergen and Department of Mathematics, University of Bergen (Sigurd.Aanonsen@cipr.uib.no)

§Department of Mathematics, University of Bergen and CIPR-Centre for Integrated Petroleum Research, University of Bergen (resme@mi.uib.no)

seismic surveys can also give information in the regions between and beyond the wells. The seismic data will in this way give information from larger parts of the spatial domain, but the frequency in time will be low. By utilising both well data and seismic data we have complementary information in the time and space domain, but the total amount of data may still be sparse because of the low frequency directions, see Figure 1.

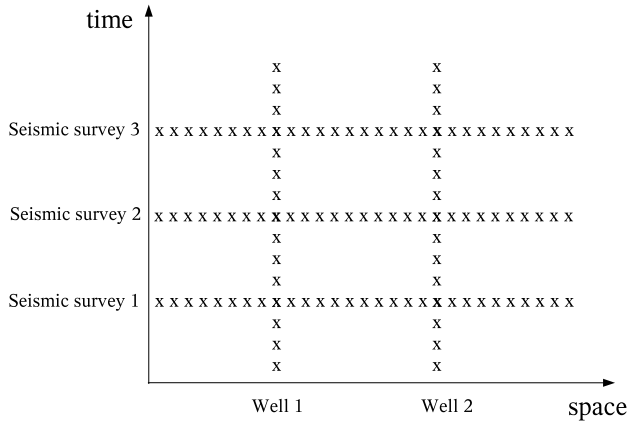


Figure 1: Distribution of measurements in time and space. The well data is sparsely distributed in space, while the time frequency is high. The seismic data have the opposite characterisation, with high frequency in space but a lower frequency in time. The two data sources give complementary information in the time and space domain, but the total amount of data may still be sparse because of the low frequency directions.

The incorporation of 4D seismic data (time-lapse data) is relatively new in history matching. A quantitative incorporation of these data has been discussed by Gosselin et.al. [1]. Aanonsen et.al [2, 3] have taken this approach further and considered the effect of using proper weights for the seismic data in the objective function.

It is well known that inverse problems often are ill-conditioned. One characteristic property of ill-conditioned problems is that even small uncertainties in the measurements can cause large errors in the solution. The sparse distribution of the data will usually make the conditioning of the inverse problem worse [4]. To reduce the risk of introducing large errors, we have to regularise the problem in a proper way. This can be done by restricting the parameter space in order to exclude non-physical solutions.

A number of methods has been applied to regularise similar inverse problems as described above. One strategy is to penalise deviations from *a priori* knowledge of the solution. This knowledge can be given by a geological model. An example of this approach is Bayesian estimation, see e.g. [5, 6]. Another strategy is to force the solution to be piecewise constant. One way to achieve this is to use a zonation, that is, dividing the domain into clusters of grid blocks, where each cluster has constant permeability. The zonation can be chosen *a priori* or it can be determined gradually through a sequence of parameter estimation problems, see e.g. [7]. In these approaches there are usually strong restrictions on the shape of the clusters of grid blocks with different constant permeability values. In [8, 9] these restrictions have been loosened by combining a multiscale zonation strategy with a level set approach.

Contrary to the referred approaches, which utilise only well data, we have in this work also incorporated seismic measurements in the observation data. As described before, the total amount of data may then be higher, and we may therefore be able to find solutions on slightly finer scales than what is searched for with only well data present.

Based on the assumption of more available information, we will in this paper propose a method where the estimation of the permeability is done directly by a level set approach, that is, without any coarse scale parameterisation method to predict an initial guess as used in [8, 9]. By the

level set formulation we restrict the estimate to be piecewise constant. The geometries of the discontinuity curves are allowed to be arbitrary, but with some forced regularity achieved by a total variation regularisation.

Level set methods can produce piecewise constant solutions with a predefined number of constant levels. If it is natural to represent the sought solution with a fewer number of regions than this predefined number, the estimate will leave one or more regions empty. In this way we only need an upper bound for the number of regions in the piecewise constant solution.

The original level set method was proposed by Osher and Sethian [10] for tracing interfaces between different phases of fluid flow. It has later been a versatile tool for representing and tracking interfaces separating a domain into subdomains. The method has been applied in a wide range of applications, i.e. inverse problems, image analysis and optimal shape design problems. For a recently survey of level set methods see [11]. Examples of level set methods applied on inverse problems can be found in [12, 13, 14, 15, 16, 17, 18, 19, 20, 21].

In this work, we shall apply a variant of a *piecewise constant level set method* [22, 23, 24, 25, 26]. In these methods the level set functions are discontinuous and have discontinuities at the boundaries of the subdomains. The method of choice is a *binary level set method*, where the level set functions are required to only take the values 1 and -1 at convergence. This method has previously been applied for segmentation of digital images [24] and for solving inverse elliptic problems [25]. Here we will apply the same framework for solving the history matching problem.

A requirement for applying the level set method on this problem is that we have indications of a piecewise constant field. The geological permeability maps can contain such information, and therefore also information about what is a suitable bound for the number of constant levels. The method presented in the theory part of this paper is a multiple level set approach able to find an arbitrary number of regions. In the numerical part we will though restrict ourselves to look at fields where we assume there are indications of a channelled system with two different levels.

The paper is organised in the following way: In Section 2 the model equations are given, and in Section 3 the inverse problem is defined. The general framework for the binary level set approach is presented in Section 4, while we in Section 5 explain how this framework is utilised to solve the inverse problem. Further the numerical optimisation method and the applied algorithm are given in Section 6. Some implementation issues are discussed in Section 7, and the numerical results are presented in Section 8. Finally the conclusions are given in Section 9.

## 2 Model Equations

Assuming only oil and water present in a porous medium with isotropic permeability, the conservation equations for two-phase incompressible, immiscible, horizontal flow are

$$\Phi(\mathbf{x}) \frac{\partial S_o}{\partial t} - \nabla \cdot \left( \frac{\kappa(\mathbf{x}) \kappa_{ro}(S_o)}{\mu_o} \nabla p_o \right) = f_o(\mathbf{x}), \quad (1)$$

$$\Phi(\mathbf{x}) \frac{\partial S_w}{\partial t} - \nabla \cdot \left( \frac{\kappa(\mathbf{x}) \kappa_{rw}(S_w)}{\mu_w} \nabla p_w \right) = f_w(\mathbf{x}), \quad (2)$$

where  $(\mathbf{x}, t) \in \Omega \times [0, T]$ .  $\Omega \in \mathbb{R}^2$  is a bounded reservoir domain and the subscripts  $o$  and  $w$  refer to the phases, water and oil, respectively.  $S_i$  denotes the saturation,  $\mu_i$  the viscosity,  $p_i$  the pressure,  $f_i$  the external volumetric flow rate and  $\kappa_{ri}$  is the relative permeability, where  $i$  is the fluid phase. The porosity and the absolute permeability are given by  $\Phi(\mathbf{x})$  and  $\kappa(\mathbf{x})$ , respectively.

In addition we assume a completely saturated medium,

$$S_o + S_w = 1, \quad (3)$$

and suppose we have a function  $P_c$  defining the capillary pressure,

$$p_o - p_w = P_c. \quad (4)$$

The quantities  $\Phi$ ,  $\kappa$ ,  $\kappa_{ri}$  and  $P_c$  are all dependent of the porous medium and are not accessible through direct measurements.

The problem treated in this paper is to find an estimate of the absolute permeability,  $\kappa(\mathbf{x})$ , when  $\Phi$  and  $\kappa_{ri}$  are assumed to be known, and  $P_c$  is set to zero. Equations (1) - (4) defines this task as an inverse problem.

### 3 The Inverse Problem

Because of the nature of the permeability it is more natural to solve the optimisation problem with respect to the logarithm of the permeability instead of the permeability itself. For notational matter we define

$$q(\mathbf{x}) = \log_{10} \kappa(\mathbf{x}), \quad (5)$$

and solve the problem with respect to  $q(\mathbf{x})$ . The transformation from  $\kappa$  till  $q$  will only influent the jumps between the different permeability zones, and not the contour of the discontinuities. This is because a piecewise constant  $\kappa$  is equivalent to a piecewise constant  $q$ . When obtaining a solution, the estimate of  $q(\mathbf{x})$  can easily be transformed back to the permeability  $\kappa(\mathbf{x})$  through Eq. (5).

Let  $\mathbf{d}_{well}$  be a vector of well data, and  $\mathbf{d}_{seis}$  be a vector of seismic data, and assume that all measurements have been tranformed into pressures and saturations:

$$\mathbf{d}_{well} = \{p_o(\mathbf{x}_{well,i}, t), S_w(\mathbf{x}_{well,i}, t) \text{ for } i = 1, 2, \dots, n_{well}, t \in [0, T]\}, \quad (6)$$

$$\mathbf{d}_{seis} = \{p_o(\mathbf{x}, t_j), S_w(\mathbf{x}, t_j) \text{ for } \mathbf{x} \in \Omega, j = 1, 2, \dots, n_{seis}\}, \quad (7)$$

where  $n_{well}$  is the number of present wells in  $\Omega$  and  $n_{seis}$  is the number of seismic surveys in the time domain  $[0, T]$ .

When incorporating different kinds of data in one optimisation process it is important to weight the different data types properly. As in [2, 3] we apply the following objective function to measure the misfit between the measured and the simulated data

$$\begin{aligned} J_{tot}(q) &= J_{well}(q) + J_{seis}(q) \\ &= \frac{1}{2}(\mathbf{d}_{well} - \mathbf{m}_{well}(q))^T D_{well}^{-1}(\mathbf{d}_{well} - \mathbf{m}_{well}(q)) + \\ &\quad \frac{1}{2}(\mathbf{d}_{seis} - \mathbf{m}_{seis}(q))^T D_{seis}^{-1}(\mathbf{d}_{seis} - \mathbf{m}_{seis}(q)). \end{aligned} \quad (8)$$

Here  $\mathbf{m}_{well}(q)$  and  $\mathbf{m}_{seis}(q)$  are the simulated values corresponding to the given measurements. These values are calculated by the forward model (Eq. (1)-(4)) for a given function  $q(\mathbf{x})$  (or corresponding permeability function  $\kappa(\mathbf{x})$ ).  $D_{well}$  and  $D_{seis}$  are the covariance matrices representing the data error.

The problem of recovering  $q(\mathbf{x})$  is an inverse problem which can be highly ill-posed. Because of the ill-posedness, a proper regularisation is required to restrict the solution space. In this work we restrict the solution to be piecewise constant. We will allow for arbitrary shapes of the geometries of the discontinuity curves, but with some restrictions related to the regularity of  $q$ . As in ([25, 13]) this is achieved by applying a total variation based regularisation together with the piecewise constant requirement. The actual applied regularisation is

$$R(q) = \int_{\Omega} |\nabla q| d\mathbf{x}, \quad (9)$$

and this will both control the length of the interfaces and the jumps of  $q$ .

The functional to be minimised is defined as

$$F(q) = J_{tot}(q) + \beta R(q), \quad (10)$$

where  $\beta > 0$  is a parameter weighting the amount of regularisation. The inverse problem is solved by finding the optimal function  $q^*$ , which is the solution of the following minimisation problem:

$$q^* = \arg \min_{q \in Q} F(q), \quad (11)$$

where  $Q$  is a space of piecewise constant functions.

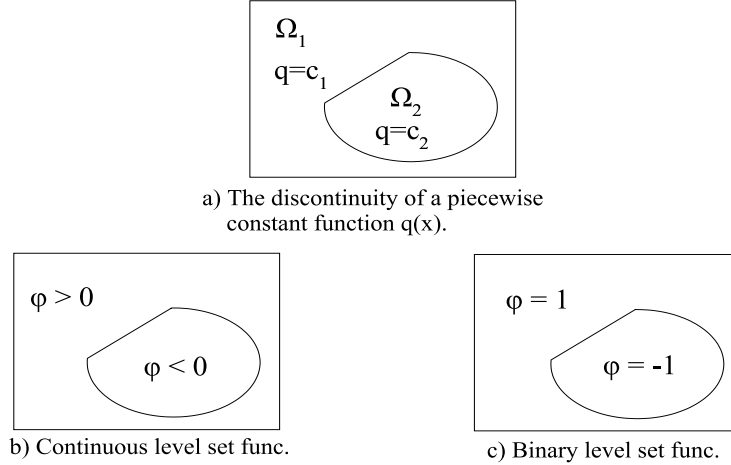


Figure 2: Level set representations of a piecewise constant function  $q(\mathbf{x})$ . In this example  $q$  has two regions with different constant values,  $c_1$  and  $c_2$ . By continuous level set functions the discontinuity of  $q$  can be represented as in Figure b), and by binary level set functions  $\phi$  is forced to take the values -1 and 1, as in Figure c).

## 4 The binary Level Set Approach

In this section we will present the binary level set formulation. The general framework for this method was first proposed in [24] where it was applied for segmentation of digital images. Some of the essential ideas for this method have appeared earlier in [27, 28]. The binary level set method has later been used in [25] for solving inverse elliptic problems. In the presented work we will follow the approach from [25] and utilise the level set functions to construct a piecewise constant coefficient function as a solution to an inverse problem. The actual inverse problem is here defined in Section 3.

In standard level set methods, continuous level set functions are used to partition a domain  $\Omega$  into a number of subdomains  $\{\Omega_j\}$ . The boundaries (or interfaces) between the subdomains are defined by the sign changes of the level set functions, and for numerical reasons the level set functions are forced to be (close to) a signed distance function. In the binary formulation, we will instead use discontinuous level set functions which at convergence should take the values -1 or 1, inside and outside the subdomains. The discontinuities of the functions will represent the boundary of the subdomains.

Let us first assume that  $\Omega$  need to be divided into two subdomains,  $\Omega_1$  and  $\Omega_2$ , such that  $\Omega_1 \cap \Omega_2 = \emptyset$  and  $\Omega = \bar{\Omega}_1 \cup \bar{\Omega}_2$ , where  $\bar{\Omega}_j$  is the closure of  $\Omega_j$ . A representation of this domain can be given by

$$\phi(\mathbf{x}) = \begin{cases} 1 & \forall \mathbf{x} \in \Omega_1 \\ -1 & \forall \mathbf{x} \in \Omega_2, \end{cases} \quad (12)$$

and the curve separating  $\Omega_1$  and  $\Omega_2$  is implicitly given as the discontinuity of  $\phi$ , see Figure 2. The properties of  $\phi$  can be used to construct a scalar function  $q(\mathbf{x})$  with distinct constant values inside the two different subdomains. If we assume that the value of  $q(\mathbf{x})$  is equal to  $c_1$  in  $\Omega_1$  and equal to  $c_2$  in  $\Omega_2$ , then  $q$  can be written as

$$q = \frac{1}{2} [c_1(\phi + 1) - c_2(\phi - 1)]. \quad (13)$$

As in the continuous level set formulation, multiple level set functions can be used to represent more than two regions. Following the terminology applied in [24], a function having four constant regions can be represented by two level set functions, and expressed as

$$q = \frac{1}{4} [c_1(\phi_1 + 1)(\phi_2 + 1) - c_2(\phi_1 + 1)(\phi_2 - 1) - c_3(\phi_1 - 1)(\phi_2 + 1) + c_4(\phi_1 - 1)(\phi_2 - 1)]. \quad (14)$$

Further,  $N$  binary level set functions can be combined to produce a coefficient function with  $2^N$  different levels. Given  $\phi = \{\phi_i\}_{i=1}^N$  and  $\mathbf{c} = (c_1, c_2, \dots, c_{2^N})$ , the function  $q$  can be expressed as the sum

$$q(\phi, \mathbf{c}) = \sum_{j=1}^{2^N} c_j \psi_j(\phi). \quad (15)$$

where  $\psi_j$  are basisfunctions dependent on  $\phi$ . An expression for  $\psi_j$  is omitted here, but can be found in [25]. Eq. (13) and Eq. (14) are special cases of Eq. (15). In the first case, we have  $\psi_1 = \frac{1}{2}(\phi + 1)$  and  $\psi_2 = -\frac{1}{2}(\phi - 1)$  in Eq. (13). With two level set functions, we get  $\psi_1 = \frac{1}{4}(\phi_1 + 1)(\phi_2 + 1)$ ,  $\psi_2 = -\frac{1}{4}(\phi_1 + 1)(\phi_2 - 1)$ ,  $\dots$  in Eq. (14).

In the following, we let  $K(x) = x^2 - 1$ . The level set functions are required to satisfy the constraint

$$K(\phi_i) = \phi_i^2 - 1 = 0 \quad \forall i. \quad (16)$$

This requirement will force the level set functions to take the values -1 or 1 at convergence. With (16) fulfilled, the basis functions will be characteristic functions for the corresponding subdomains, i.e.  $\psi_j = 1$  in  $\Omega_j$  and zero elsewhere. That is, the support of the different basis functions are non-overlapping,  $\text{supp } \psi_i \cap \text{supp } \psi_j = \emptyset \quad \forall i \neq j$ , and the total support of all the basisfunctions covers the complete domain, i.e.  $\Omega = \cup_{j=1}^{2^N} \text{supp } \psi_j$ .

## 5 The Binary Level Set Method for the Inverse Problem

From the last section, we see that every piecewise constant function can be represented as in (15) under the requirement that the level set functions satisfy (16). In order to find a piecewise constant function, we just need to find the corresponding  $c_j$ -values and the level set functions  $\phi_i$ . If we define the vector  $\mathbf{K}(\phi) = \{K(\phi_i)\}_{i=1}^N$ , we can thus reformulate problem (11) as

$$(\phi^*, \mathbf{c}^*) = \arg \left\{ \min_{\phi, \mathbf{c}} F(q(\phi, \mathbf{c})) \quad \text{subject to} \quad \mathbf{K}(\phi) = \mathbf{0} \right\}, \quad (17)$$

where the optimal coefficient can be calculated by  $q^* = q(\phi^*, \mathbf{c}^*)$ . The constraint  $\mathbf{K} = \mathbf{0}$  is applied to control the structure of the level set functions, and will therefore depend on the choice of basis functions.

Define  $\tilde{F}(\phi, \mathbf{c}) = F(q(\phi, \mathbf{c}))$ . To evolve the level set functions and update the constant values such that  $q(\mathbf{x})$  will converge to the optimal solution, we need to calculate the derivatives of  $\tilde{F}$  with respect to  $\phi$  and  $\mathbf{c}$ . By the chain rule we have, c.f. [13],

$$\frac{\partial \tilde{F}}{\partial \phi_i} = \frac{\partial F}{\partial q} \frac{\partial q}{\partial \phi_i} \quad \forall i = 1, 2, \dots, N \quad (18)$$

and

$$\frac{\partial \tilde{F}}{\partial c_j} = \int_{\Omega} \frac{\partial F}{\partial q} \frac{\partial q}{\partial c_j} dx \quad \forall j = 1, 2, \dots, 2^N. \quad (19)$$

The time consuming part of these calculations is to find  $\frac{\partial F}{\partial q}$ . In this work  $\frac{\partial F}{\partial q}$  is calculated by adjoint gradient calculations (see e.g. [29]) in a reservoir simulator.

## 6 Numerical Optimisation

We apply an augmented Lagrangian method to solve problem (17) numerically. The Lagrangian functional involves both  $\tilde{F}$  and the constraint  $K$ ;

$$L(\phi, \mathbf{c}, \boldsymbol{\lambda}) = \tilde{F}(\phi, \mathbf{c}) + \sum_{i=1}^N \int_{\Omega} \lambda_i K(\phi_i) dx + \mu_p \sum_{i=1}^N \int_{\Omega} |K(\phi_i)|^2 dx. \quad (20)$$

Here  $\mu_p > 0$  is a penalisation parameter which usually is a fixed parameter chosen *a priori*, or it can in some cases be increased carefully through the iterations to improve the convergence.  $\boldsymbol{\lambda} = \{\lambda_i\}_{i=1}^N$  is the Lagrangian multipliers where  $\lambda_i$  is a function defined in the same domain as  $\phi_i$ .

We search a saddle point of  $L$  and therefore require

$$\frac{\partial L}{\partial \phi_i} = 0, \quad \frac{\partial L}{\partial \lambda_i} = 0 \quad \forall i \in \{1, \dots, N\} \quad \text{and} \quad \frac{\partial L}{\partial c_j} = 0 \quad \forall j \in \{1, \dots, 2^N\}. \quad (21)$$

Starting with initial guesses  $\phi^0$ ,  $\mathbf{c}^0$  and  $\boldsymbol{\lambda}^0$ , we iterate towards the better approximations denoted by  $\phi^k$ ,  $\mathbf{c}^k$  and  $\boldsymbol{\lambda}^k$  where  $k = \{1, 2, \dots\}$ . These variables are updated using a steepest descent method, and when the change of the variables approach zero, the iterations can be stopped. Expressions of the gradients in (21) and a more detailed description of the numerical updates can be found in [25]. In [26] a MBO operator splitting scheme has been applied for solving related problems.

Because of the computationally effort to run the forward model, we have in this work applied a fixed timestep when updating  $\phi$  instead of the line search applied in [25]. The updating of each  $c_j$  is less stable than the updating of  $\phi$ , so to update  $\mathbf{c}$  we have used separate line searches for each  $c_j$  to prevent choosing timesteps that will increase the value of  $\tilde{F}$ . The actual applied algorithm is as follows:

**Algorithm A** (Uzawas Algorithm for Variational Level Set Methods)

Determine how many level set functions,  $N$ , to use.

Choose timestep for  $\phi$ :  $\Delta t_\phi$ .

Choose search interval for each  $c_j$ :  $c_j \in [a_j, b_j]$ .

Initialise:  $\phi^0$ ,  $\mathbf{c}^0$  and  $\boldsymbol{\lambda}^0$  and set  $k = 0$ .

1. Update  $\phi$ ;

(a) Compute  $q$  by Eq. (15).

(b) Evolve the level set functions:  $\phi^{k+1} = \phi^k - \Delta t_\phi \frac{\partial L}{\partial \phi}(\phi^k, \mathbf{c}^k, \boldsymbol{\lambda}^k)$ .

2. Update  $\mathbf{c}$  (after a fixed number of iterations);

For each  $c_j$ ,  $j = 1, 2, \dots, 2^N$ :

(a) Compute  $q$  by Eq. (15).

(b) Define:  $\alpha_{c_j}^k = \frac{\partial L}{\partial c_j}(\phi^{k+1}, \mathbf{c}^k, \boldsymbol{\lambda}^k)$ .

(c) Define the search interval: Let  $M \in \mathbb{R}$  be all values of  $\Delta t$  such that  $c_j^k - \Delta t \alpha_{c_j}^k \in [a_j, b_j]$ .

(d) Find the optimal timestep:  $\Delta t_{c_j} = \arg \min_{\Delta t \in M} L(\phi^{k+1}, \mathbf{c}^k - \Delta t \alpha_{c_j}^k \mathbf{e}_j, \boldsymbol{\lambda}^k)$ , where  $\mathbf{e}_j$  is the  $j$ 'th unit vector.

(e) Update this constant:  $c_j^{k+1} = c_j^k - \Delta t_{c_j} \alpha_{c_j}^k$ .

3. Update  $\boldsymbol{\lambda}$  (after a fixed number of iterations);

$$\boldsymbol{\lambda}^k = \boldsymbol{\lambda}^k + \mu \mathbf{K}(\phi^{k+1}).$$

4. Iterate again if necessary;

$$k = k + 1.$$

Notice that  $q$  is updated implicitly using the most recently calculated values of  $\phi$  and  $\mathbf{c}$ . In this algorithm we do not use step 2 and 3 in every iteration. This is because the algorithm becomes unstable if  $\mathbf{c}$  and  $\boldsymbol{\lambda}$  are updated too often. In principle we could have run step 1 to convergence before doing the other steps. Numerically this is not strictly necessary and it would have been computationally heavy. We have therefore updated  $\mathbf{c}$  and  $\boldsymbol{\lambda}$  after a fixed numbers of iterations.

## 7 Implementation Issues

As is typical for Augmented Lagrangian algorithms, the convergence is fast in the beginning and it slows down when the solution is getting closer to the true minimiser. A natural remedy to this, is to apply larger timesteps when evolving  $\phi$ , but this will make the algorithm unstable. Another problem, when solving inverse problems, is that the sensitivities related to changes in the data with respect to  $q$  may be very small in some regions. This will further slow down the speed of convergence.

As in [25] we have used a modification of the original binary level set function to speed up the convergence of the method. When computing  $q = q(\phi, \mathbf{c})$  we have replace each  $\phi_i$  by the function

$$\tilde{\phi}_i = \text{sgn}(\phi_i) = \begin{cases} \frac{\phi_i}{|\phi_i|} & \text{for } \phi_i \neq 0, \\ 0 & \text{else.} \end{cases} \quad (22)$$

We define the vector  $\tilde{\phi} = \{\tilde{\phi}_i\}_{i=1}^N$ , and then replace  $\phi$  by  $\tilde{\phi}$  when calculating  $q$  in Eq. (15). By the chain rule we have

$$\frac{\partial q}{\partial \phi_i} = \frac{\partial q}{\partial \tilde{\phi}_i} \frac{\partial \tilde{\phi}_i}{\partial \phi_i} = \frac{\partial q}{\partial \tilde{\phi}_i} \delta(\phi_i), \quad (23)$$

where  $\delta$  denotes the delta Dirac function, i.e.  $\delta(0) = 1$  and  $\delta(\phi_i) = 0 \forall \phi_i \neq 0$ .

In numerical implementations, it is desirable to replace  $\tilde{\phi}_i$  by a smoothed approximation. The chosen approximation is

$$\tilde{\phi}_i \approx \frac{\phi_i}{\sqrt{\phi_i^2 + \epsilon}}, \quad (24)$$

where  $\epsilon$  is a small positive number which has to be chosen. As  $\phi_i$  is replaced by  $\tilde{\phi}_i$ , the gradient calculation in (18) and (19) also needs to be changed using (23). However, in [25] it was observed that good results were obtained if we just replace  $\delta(\phi_i)$  in (23) by 1. That approach is also applied in this work. A numerical study of the improvement related to the speed of the modified algorithm, and a more thorough discussion of the advantages of this approach can be found in [25].

By numerical experiments we have found it desirable to start with a rather large value of  $\epsilon$ , and then decrease  $\epsilon$  during the iterations. In this setting it is also natural to increase  $\mu_p$  during the iterations. This differs from other related works [24, 23, 13], where a fixed  $\mu_p$  has been used to reduce the ill-conditionness of the problem.

The minimisation with respect to  $\mathbf{c}$  is a highly ill-conditioned process. It should therefore not be done too early or too frequently during the iterations. To further stabilise this process, we have applied a predefined search interval  $[a_j, b_j]$  for each constant such that there will be no risk of producing values completely out of range.

The applied method is searching a piecewise constant solution with a predefined number of constant values. For practical applications it may be desirable to stop the algorithm before the solution is strictly piecewise constant. The obvious advantage with this is that the change in the solution may be very small towards the end of the optimisation, and therefore, stopping at an earlier stage will produce approximately the same solution within less time. In a real field, we do not know if there are sharp discontinuities between the regions, and if this should be the case, these sharp discontinuities will probably not match the simulator grid perfectly.

We have found it difficult to find any suitable stopping criterion which will stop the iterations before the solution is strictly piecewise constant. In this work we will run the algorithm to a fixed number of iterations, or till both  $\phi$  and  $\mathbf{c}$  have stopped changing.

## 8 Numerical Results

In this section we will present some numerical examples where we study the performance of the presented method. The studied examples are synthetic cases where the true permeability field consists of two distinct permeability values. With two different permeability values, it is sufficient with one level set function to represent the field. The test reservoir is square and horizontal with

constant thickness and no-flow outer boundaries. Except for the absolute permeability, the fluid and rock properties are held fixed through the simulations. In the field we have one injector positioned in the lower left corner, and one producer positioned in the upper right corner.

The relative permeability functions are defined by the Corey models;

$$\begin{aligned}\kappa_{rw} &= \hat{\kappa}_{rw} \left( \frac{S_w - S_{wr}}{1 - S_{wr} - S_{or}} \right)^{e_w}, \\ \kappa_{ro} &= \hat{\kappa}_{ro} \left( \frac{S_o - S_{or}}{1 - S_{or} - S_{wr}} \right)^{e_o},\end{aligned}$$

where the Corey exponents,  $e_w$  and  $e_o$ , the residual saturations,  $S_{wr}$  and  $S_{or}$ , and the endpoint permeabilities,  $\hat{\kappa}_{rw}$  and  $\hat{\kappa}_{ro}$ , are assumed known. The numerical values for these properties are, together with the rest of the properties for the simulations, listed in Table 1.

Reservoir dimensions:	1000 × 1000 × 40 meter	
Simulation grid:	16 × 16 × 1 cells	
Porosity:	0.2	
Viscosity:	$\mu_w = 0.5 \cdot 10^{-3} \text{ Pa} \cdot \text{s}$	$\mu_o = 0.5 \cdot 10^{-3} \text{ Pa} \cdot \text{s}$
Endpoint relative permeabilities:	$\hat{\kappa}_{rw} = 0.1$	$\hat{\kappa}_{ro} = 1$
Residual saturations:	$S_{rw} = 0.2$	$S_{or}^* = 0.2$
Corey exponents:	$e_w = 1.5$	$e_o = 2.5$
Initial saturation:	$S_w = 0.2$	$S_o = 0.8$
Capillary pressure function:	$P_c(S_w) \equiv 0 \text{ kPa}$	
Injection rate:	8% of total pore volume per year.*	
Production rate:	constant BHP = 200.0 bar	
Number of timesteps:	192	
Total production time:	3000 days	
Number of seismic surveys:	16 (i.e. approximately every 6 months.)	

Table 1: Properties for the simulations. \*In Example 5 the injection rate is changed to 3.5% of total pore volume per year.

The forward model (the solution of Eq. (1)-(4) for a given function  $q(\mathbf{x})$ ) is solved by applying an in-house reservoir simulator. In the simulator the equation error is minimised by applying Newton iterations, and the linear solver of choice is GMRES. The gradients,  $\frac{\partial F}{\partial q}$ , are obtained from the solution of the adjoint system of equations, see e.g. [29].

For each reference permeability field we calculate the true values of saturation ( $S_w$ ) and pressure ( $p_o$ ) for the applied timesteps on the given grid. Thereafter synthetic measurements are constructed by adding noise to the calculated true values. The noise is assumed to be uncorrelated Gaussian noise with zero mean. In Table 2 the standard deviations which give the amount of added noise are listed. Notice that the uncertainties are larger for the seismic measurements than for the measurements in the wells. When calculating  $J_{tot}(q)$  we use the correct uncertainties, according to the added noise, for constructing  $D_{well}$  and  $D_{seis}$ .

	Well data	Seismic data
Pressure	$\sigma_{p,well} = 1.0 \text{ bar}$	$\sigma_{p,seis} = 2.5 \text{ bar}$
Saturation	$\sigma_{S,well} = 0.025$	$\sigma_{S,seis} = 0.050$

Table 2: Standard deviations for the added noise. The noise is larger for the seismic data than for the well data.

The penalisation parameter  $\mu_p$  is increased slowly through the iterations. If  $k$  is the number of iterations,  $\mu_p = 0.05 \cdot 1.01^k$  up till it reaches an upper bound (equal to 4) where we keep it fixed. Regarding the regularisation parameter  $\beta$ , we have for each example first tried with a value of  $5 \cdot 10^{-3}$ . If this causes large oscillations in the solution, then the weight on the regularisation is increased and a new optimisation is performed. The value of  $\epsilon$  used to calculate  $\tilde{\phi}$  is initially equal

to 0.1, and is decreased by a factor of 0.98 until it reaches a lower bound equal to  $10^{-7}$ . Both the Lagrangian parameter  $\lambda$  and the  $c_j$ -values are updated each  $10^{\text{th}}$  iteration.

For each test case we start with  $\phi^0 = 0$  in the entire domain except in the cells where we have wells. An initial  $\phi^0 = 0$  means that we do not assume anything about the contour of the discontinuity. In the cells with a penetrating well, we assume that the approximate permeability value is known. The value of  $\phi$  is therefore fixed equal to its correct value (-1 or 1 dependent of the initial  $\mathbf{c}$ -value) in these cells.

For each of the constant values we define an interval  $[a_j, b_j]$  within  $c_j$  should be estimated. The length of this interval will correspond to the *prior* uncertainty of the permeability value for the corresponding region. Because there are abilities for direct measurements of the permeability in the wells, we have applied a lower uncertainty for  $c_j$  in the regions where there is at least one well present, than for the regions with no wells. For the studied cases we have applied intervals  $[a_j, b_j]$  with length equal 50% (no wells) and 30% (wells) of the difference between the two true values of  $q$ . The centre of the intervals are chosen equal to the true values. For example, if we assume the following;  $c_1$  and  $c_2$  are the true values, the region corresponding to  $c_1$  has no wells present and there are one or more wells penetrating a region with permeability approximately equal to  $c_2$ . Then the bounds will be

$$a_1 = c_1 - 0.25 \cdot |c_2 - c_1|, \quad b_1 = c_1 + 0.25 \cdot |c_2 - c_1|$$

and

$$a_2 = c_2 - 0.15 \cdot |c_2 - c_1|, \quad b_2 = c_2 + 0.15 \cdot |c_2 - c_1|.$$

In this work we start with initial  $c_j$ -values on the lower and upper bound of the two intervals. We use the lower bound for the smallest  $c_j$ -value and the upper bound for the highest  $c_j$ -value, that is, if  $c_1 < c_2$ , then  $c_1^0 = a_1$  and  $c_2^0 = b_2$ . Other approaches for choosing the initial values are also possible.

The algorithm is stopped after 1000 iterations if  $\phi^k$  and  $\mathbf{c}^k$  have not converged, in the sense of stopped changing, before this.

For each studied example we have plotted measures of the errors and the convergence. One of the measures is the equation error. We define  $e_o(q, p_o, S_w)$  and  $e_w(q, p_o, S_w)$  to be the equation residual for Eq. (1) and (2), respectively, and let the equation error

$$E(q, p_o, S_w) = \sum_{i=o,w} \|e_i(q, p_o, S_w)\|_{L_2(\Omega \times [0, T])}. \quad (25)$$

Since Eq. (1) and (2) are solved exactly in the forward model, the residual  $E(q^k, m(q^k))$  should be zero or below a numerical error bound. To produce a measure of the amount of change in the solution in one iteration, we have calculated  $E(q^k, m(q^{k-1}))$ . Plotting corresponding equation errors versus iteration number can, even for linear equations (see [13]), produce highly oscillating curves. For non-linear equations the situation can be even worse. To easier detect the trend of these curves, we have also plotted a moving average of the  $E(q^k, m(q^{k-1}))$ . For the calculation of the moving average, we have used an average of the last 15 values of  $E(q^k, m(q^{k-1}))$ .

To measure the data fit we plot RMS values of  $J$ ,  $J_{well}$  and  $J_{seis}$  versus the iteration number. The RMS value of a function  $J_\alpha$  is defined as  $\sqrt{2J_\alpha/n_\alpha}$ , where  $n_\alpha$  is the number of measurements included in  $J_\alpha$  and  $\alpha = tot, well$  or  $seis$ .

Other measures applied to check the convergence are  $\|K(\phi^k)\|_{L_2}$  and  $\|K(\tilde{\phi}^k)\|_{L_2}$ . The difference between these two measures is that the first one indicates how fast  $\phi^k$  reaches the convergence values -1 and 1, and the second one is a measure of how close  $\hat{q}^k$  is from being piecewise constant with only two levels.

### Example 1: S-shaped Channel

In this example the true field is an S-shaped channel with high permeability from the injector till the producer. A plot of the field is shown in Figure 3a), while the true discontinuity curve of the permeability is plotted in Figure 3b). In this field there are three distinct piecewise constant

regions, but since two of the regions have the same constant value, *one* level set function is sufficient to give a representation of it. This is related to the level set methods' nice feature of splitting and merging regions independent of their contours (see for example [11]).

In Figure 4 the development of the estimates  $q^k$  and the signchange of  $\phi^k$  are shown. Already after 50 iterations the estimate is quite close to the true field, but we need approximately 200 iterations to produce a field which is piecewise constant with only two levels. From this time the solution stops changing.

Error measures and convergence curves are shown in Figure 5. If we compare the different curves, we observe that the RMS functions (Fig. 5c)) are decreasing much faster and for a shorter period than what is the case for all the other functions. After the initial rapid decrease, the RMS functions reach a stable value just above 1. The other measures are also reaching stable values, but after a higher number of iterations. Notice that the RMS functions are plotted in semilogarithmic scale, while most of the other functions (not the the equation residuals) are given in linear plots. This makes the difference in the behaviour of the curves even more clear.

The rapid decrease in the RMS functions can usually be explained by low sensitivities with respect to the permeability changes in some areas of the field. The sought solution may therefore be difficult to find, and the convergence can be very slow towards the end of the optimisation. The described phenomenon can be observed in all the tested examples and illustrates the ill-posedness of the treated inverse problem.

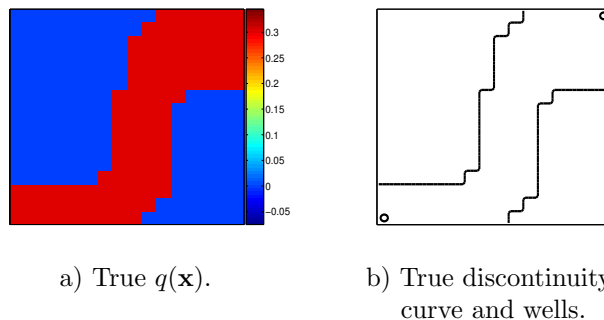


Figure 3: Example 1: True permeability and the corresponding discontinuity. The constant levels are given by  $\mathbf{c} = (0, 0.3)$ , which corresponds to a permeability equal to 1 D and 2 D. The circles in the corners are indicating the positioning of the wells.

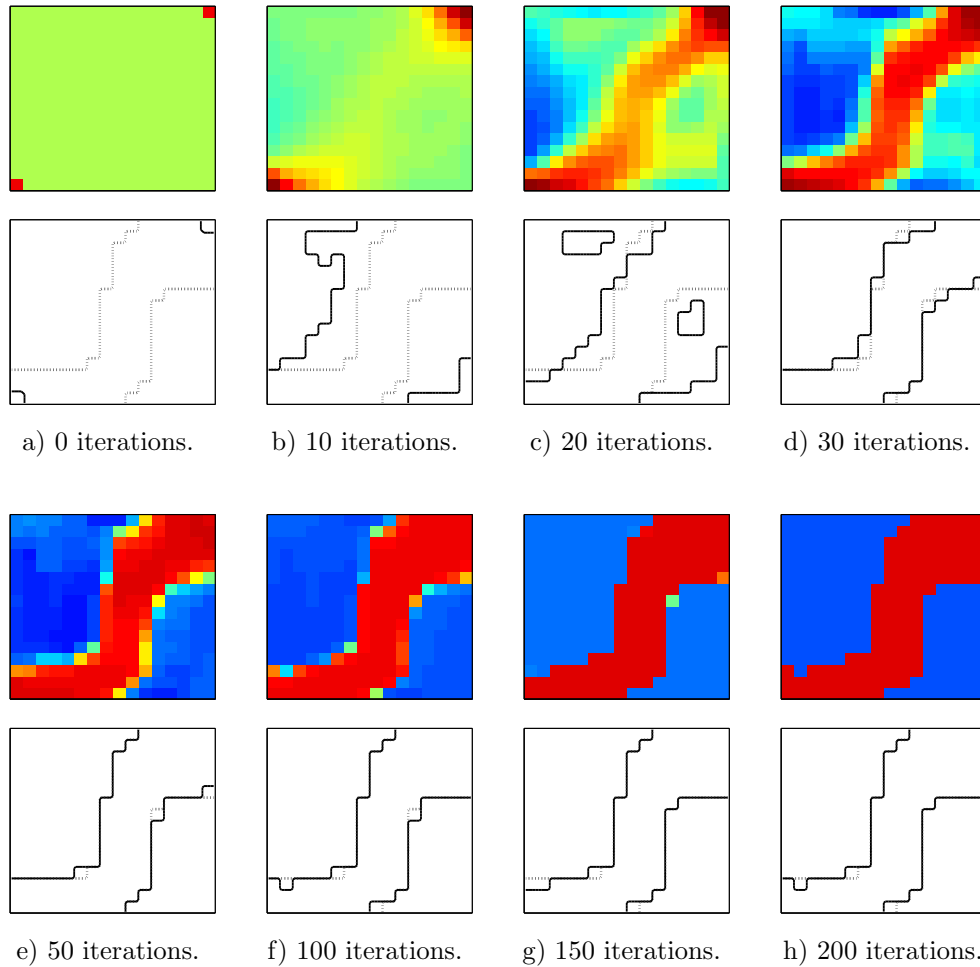


Figure 4: Example 1: The estimated permeability for different iterations. In the upper rows  $q^k$  is plotted with the same colourmap as used in Figure 3a). In the lower rows the signchanges of  $\phi^k$  are shown by the solid lines, and the discontinuities of the true  $q(\mathbf{x})$  are given by the dotted lines. Initially  $\phi^0 = 0$  in the entire domain, except in the corners where the wells are located. In the intermediate iterations the values of  $\phi^k$  will evolve towards -1 or 1 in the different parts of the domain. After about 50 iterations the true field is approximately matched. We though need about 200 iterations before  $\phi^k$  is (approximately) equal to 1 or -1 in all cells, and at this stage the field is piecewise constant with only two levels.

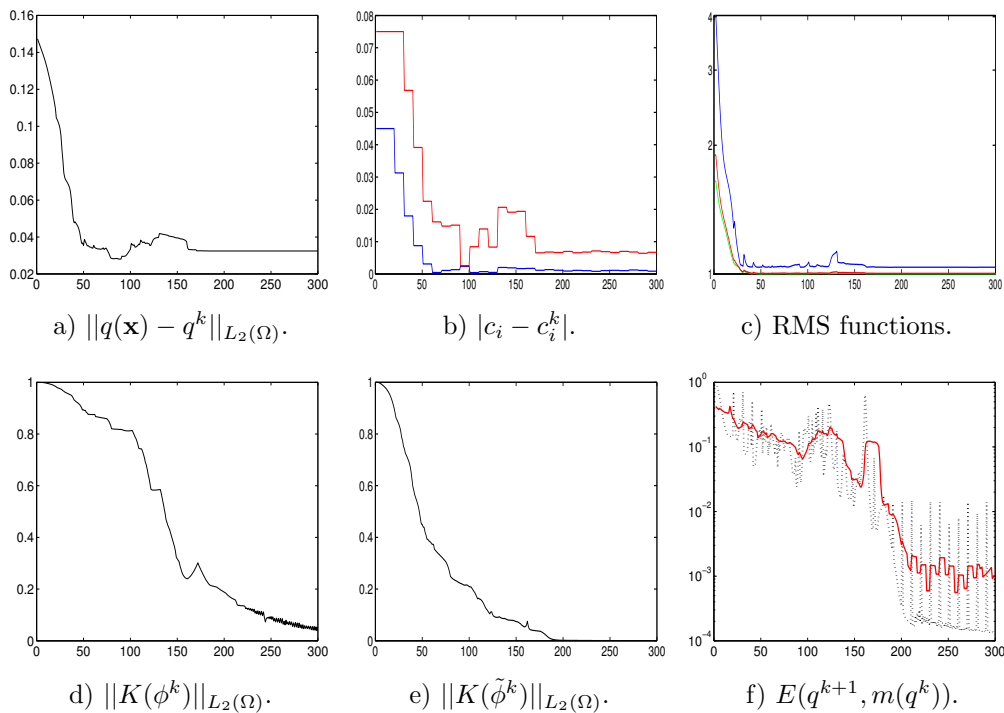


Figure 5: Example 1. Error measures and convergence plots versus the iteration number. Figure a) and b) give the error in the computed  $q^k$  and  $c_j^k$ -values. In Figure c) the red curve gives the RMS values of  $J_{tot}$ , while the blue and the green curves are the RMS functions for  $J_{well}$  and  $J_{seis}$ , respectively. Measures of the convergence of  $\phi^k$  and  $\tilde{\phi}^k$  are shown in Figure d) and e), respectively, while  $E(q^{k+1}, m(q^k))$  in Figure f) is the norm of the equation residual. The red curve in Figure f) is an average of  $E(q^{k+1}, m(q^k))$  for the last 15 iterations. The curves indicate convergence after about 200 iterations.

## Example 2: Horizontal Barrier

In this example the true field is a horizontal barrier with low permeability across the entire field. The inflow from the injector has to cross this barrier to reach the producer, see Figure 6.

From the recovered  $q^*$  given in Figure 7 d) we observe that the contour of the discontinuity is matching most of the main structures of the true field, but there are also some larger errors. Errors in the geometry of the discontinuities are typically related to errors also in the constant values (plotted in Fig. 8b)). In this case the error in the  $c_j$ -value corresponding to the low permeable region is not reduced significantly from the initial value. We can also observe large oscillations in the equation residual (Fig. 8f)), and that the constraint  $\|K(\phi^k)\|_{L_2(\Omega)}$  (Fig. 8d)) is not decreasing monotonically towards zero. This behaviour can sometimes occur when the method has large difficulties in finding a stable piecewise constant solution which reconcile the data.

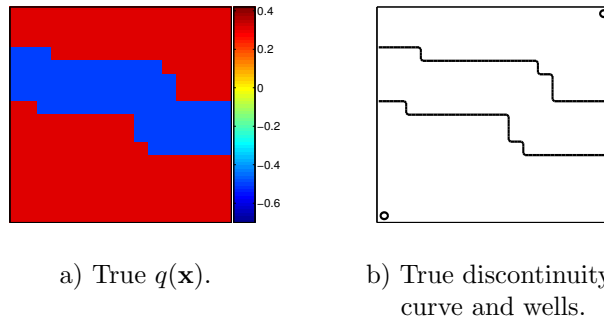


Figure 6: Example 2: True permeability and the corresponding discontinuity. The constant levels are given by  $\mathbf{c} = (-0.5, 0.3)$ , which corresponds to a permeability equal to 316 mD and 2 D. The circles in the corners are indicating the positioning of the wells.

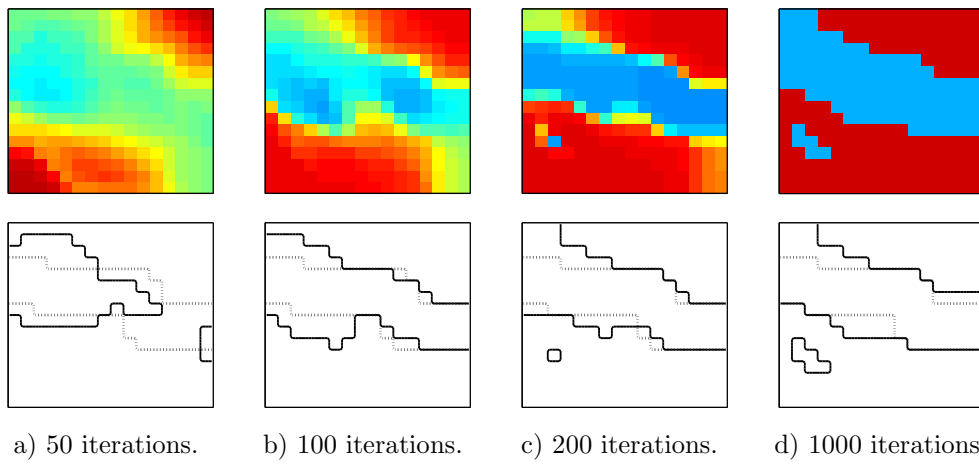


Figure 7: Example 2: The estimated permeability for different iterations. In the upper figures  $q^k$  is plotted with the same colourmap as used in Figure 6a). In the lower figures the signchanges of  $\phi^k$  are shown by the solid lines, and the discontinuities of the true  $q(\mathbf{x})$  are given by the dotted lines.

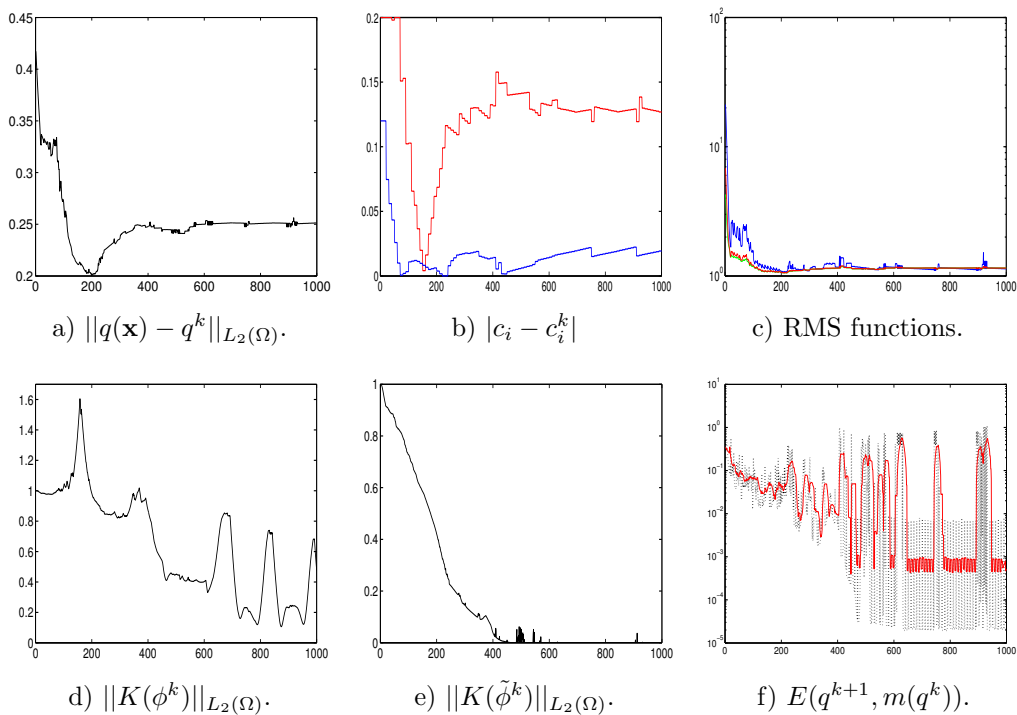


Figure 8: Example 2. Error measures and convergence plots versus the iteration number. Figure a) and b) give the error in the computed  $q^k$  and  $c_j^k$ -values. In Figure c) the red curve gives the RMS values of  $J_{tot}$ , while the blue and the green curves are the RMS functions for  $J_{well}$  and  $J_{seis}$ , respectively. Measures of the convergence of  $\phi^k$  and  $\tilde{\phi}^k$  are shown in Figure d) and e), respectively, while  $E(q^{k+1}, m(q^k))$  in Figure f) is the norm of the equation residual. The red curve in Figure f) is an average of  $E(q^{k+1}, m(q^k))$  for the last 15 iterations.

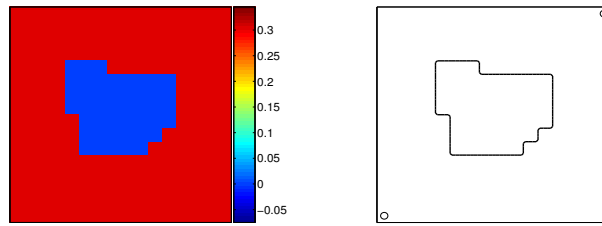
### Example 3: Centred low permeable Region

This example illustrates the recovery of a region with lower permeability in a region positioned in the middle of the field. The true field is shown in Figure 9.

The solution plotted in Figure 10 gives a field with lower permeability in approximately the correct region. The produced region with the lowest permeability is though not connected, and the shape is different from the true solution. In spite of the error in the contour of the recovered region, the relative errors of the constant values  $c_j^k$  is low (Fig. 11 b)).

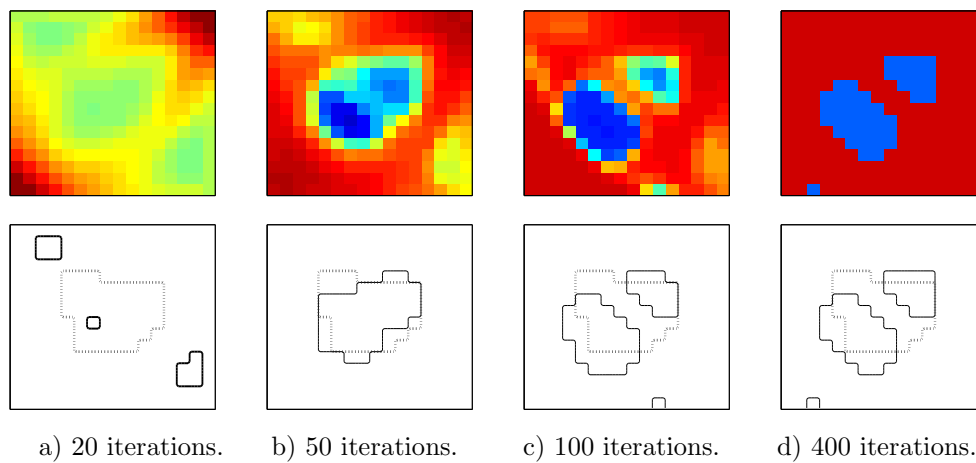
For this example, we do not observe the same kind of oscillations or artifacts in the convergence plots (Fig. 11) as was the case for Example 2. The increase in  $\|K(\phi^k)\|_{L_2(\Omega)}$  (Fig. 11e)) in the early stages is because  $|\phi^k|$  is getting much larger than 1 in some regions of the domain. This may happen when the Lagrangian multiplier,  $\lambda$ , is close to zero and the weight of the constraint, controlled by  $\mu_p$ , is low. Later in the process, when these controlling terms get a higher weight,  $\|K(\phi^k)\|_{L_2(\Omega)}$  starts to decrease towards zero as expected.

The error of  $q^k$  (Fig. 11a)) has its lowest value at around 50 iterations. At this point the solution is not piecewise constant, but has smooth connections between the regions (Fig. 10a)). The optimisation method is only searching solutions which are piecewise constant with two regions. In this case the error in the solution is increasing when the constraint  $K(\phi) = 0$  is weighted higher and by this forcing the solution to be piecewise constant. Similar behaviour can also be observed in some of the other studied examples.

a) True  $q(\mathbf{x})$ .

b) True discontinuity curve and wells.

Figure 9: Example 3: True permeability and the corresponding discontinuity. The constant levels are given by  $\mathbf{c} = (0, 0.3)$ , which corresponds to a permeability equal to 1 D and 2 D. The circles in the corners are indicating the positioning of the wells.



a) 20 iterations.

b) 50 iterations.

c) 100 iterations.

d) 400 iterations.

Figure 10: Example 3: The estimated permeability for different iterations. In the upper figures  $q^k$  is plotted with the same colourmap as used in Figure 9a). In the lower figures the signchanges of  $\phi^k$  are shown by the solid lines, and the discontinuities of the true  $q(\mathbf{x})$  are given by the dotted lines. A solution close to the true field is achieved after about 50 iterations, but this field is not fulfilling the piecewise constant requirement.

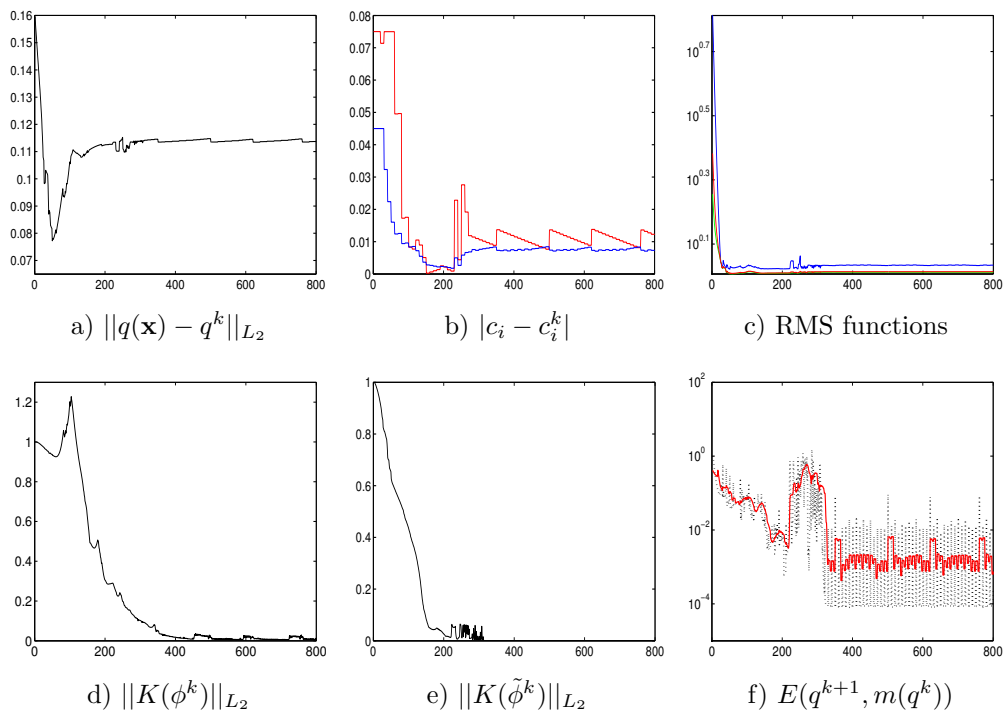


Figure 11: Example 3. Error measures and convergence plots versus the iteration number. Figure a) and b) give the error in the computed  $q^k$  and  $c_j^k$ -values. In Figure c) the red curve gives the RMS values of  $J_{tot}$ , while the blue and the green curves are the RMS functions for  $J_{well}$  and  $J_{seis}$ , respectively. Measures of the convergence of  $\phi^k$  and  $\tilde{\phi}^k$  are shown in Figure d) and e), respectively, while  $E(q^{k+1}, m(q^k))$  in Figure f) is the norm of the equation residual. The red curve in Figure f) is an average of  $E(q^{k+1}, m(q^k))$  for the last 15 iterations. The curves indicate convergence after about 400 iterations.

#### Example 4: System of Channels - low Contrast

This example involves a more complicated field where two channels are crossing each other (see Fig. 12). The two channels are assumed to have the same permeability value, and together they produce a connected region with high permeability from the injector to the producer.

The estimates  $q^k$  and the sign of  $\phi^k$  are shown for different iteration numbers in Figure 13, and the convergence is shown in Figure 14. Even with this complicated geometry, the level set method is able to recover the constant levels and the geometry of the discontinuities with a relatively low error. In the final solution, one of the branches of the channels is not connected to the rest of the system and the fine details of the discontinuity lines are not matched exactly. Though, the main structures of the field are recovered very well.

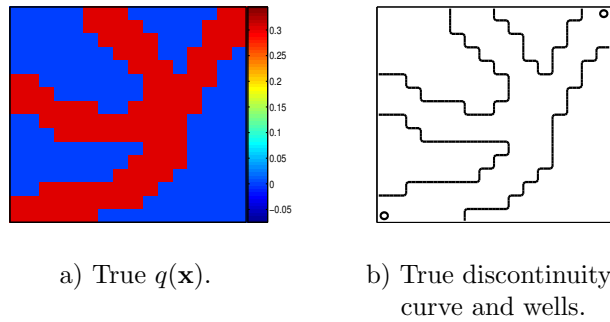


Figure 12: Example 4: True permeability and the corresponding discontinuity. The constant levels are given by  $\mathbf{c} = (0, 0.3)$ , which corresponds to a permeability equal to 1 D and 2 D. The circles in the corners are indicating the positioning of the wells.

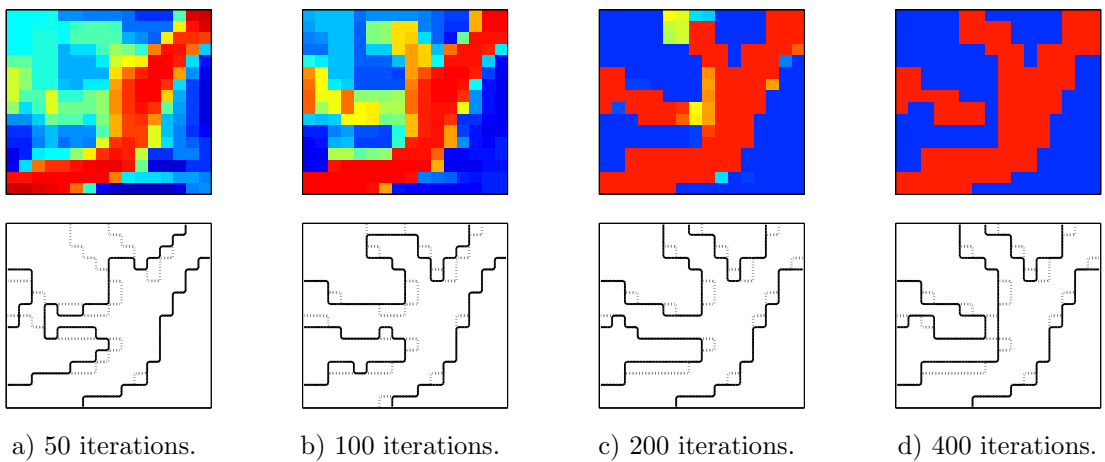


Figure 13: Example 4: The estimated permeability for different iterations. In the upper figures  $q^k$  is plotted with the same colourmap as used in Figure 12a). In the lower figures the signchanges of  $\phi^k$  are shown by the solid lines, and the discontinuities of true  $q(\mathbf{x})$  are given by the dotted lines.

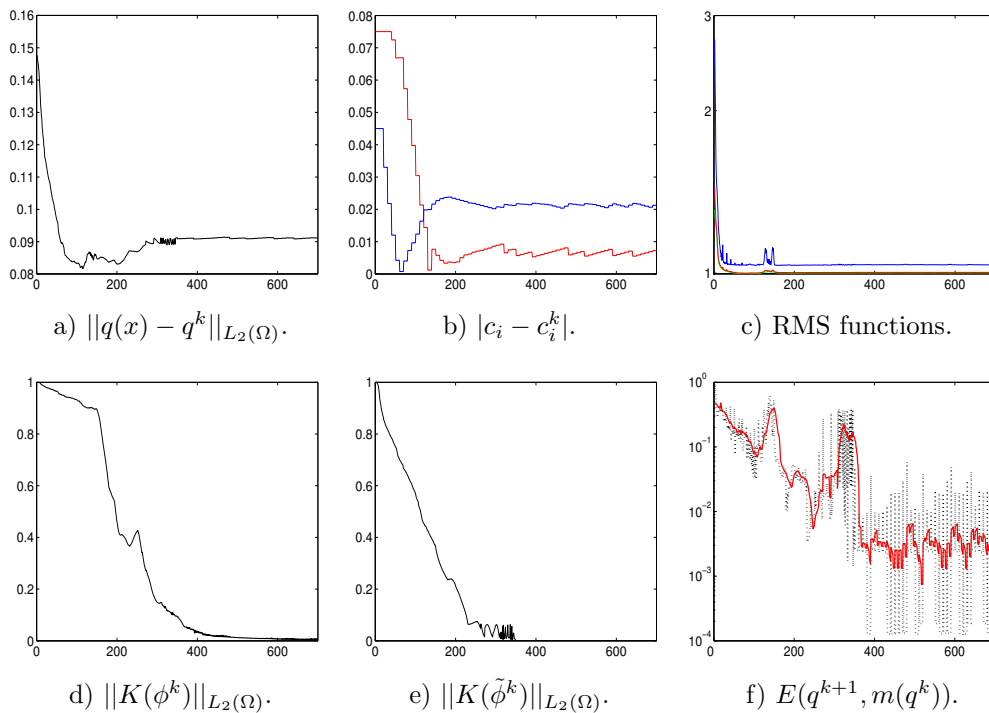


Figure 14: Example 4. Error measures and convergence plots versus the iteration number. Figure a) and b) give the error in the computed  $q^k$  and  $c_i^k$ -values. In Figure c) the red curve gives the RMS values of  $J_{tot}$ , while the blue and the green curves are the RMS functions for  $J_{well}$  and  $J_{seis}$ , respectively. Measures of the convergence of  $\phi^k$  and  $\tilde{\phi}^k$  are shown in Figure d) and e), respectively, while  $E(q^{k+1}, m(q^k))$  in Figure f) is the norm of the equation residual. The red curve in Figure f) is an average of  $E(q^{k+1}, m(q^k))$  for the last 15 iterations. The curves indicate convergence after about 400 iterations.

### Example 5: System of Channels - high Contrast

The true field, plotted in Figure 15, is in this case equal to the field in Example 4 except that the constant values of the permeability in the two regions are changed. We have now a higher contrast between the two permeability values, and in addition, the lowest permeability value (equal to 32 mD) is here much lower than the corresponding permeability in the previous example (equal to 1 D). Because of the less permeable field, the constant injection rate per year is reduced to 3.5% of total pore volume for this example.

The results in Figure 16 show that we are capturing a high permeable channel from the injector till the producer, but the other branches of the channels are not discovered. In some of the convergence plots in Figure 17 we can observe large oscillations. This illustrates the difficulties of producing a piecewise constant field as a solution to this problem. The relative reduction in the error of  $q^k$  (Fig. 17a)) is quite small for this example. This can be explained by the misclassification of some parts of the channels. The misclassified parts are by the method classified as low permeable regions, which in fact is less close to the true solution than the initial guess. The initial value,  $q^0$ , is (except for the cells with wells) equal to the mean of  $c_1^0$  and  $c_2^0$  (given by  $\phi = 0$  in Eq. (13)).

In Figure 18 we have compared the simulated seismic data for the true fields used in Example 4 (low contrast) and Example 5 (high contrast). We have plotted  $p_o$  and  $S_w$  at the end of the simulations.

The plots of  $S_w$  show that for Example 4 the entire field will be flooded by water, while in Example 5, the main part of the flow will go in the high permeable region discovered by the level set method. In the last case, the flow will move very slowly in the low permeable regions and also in the parts of the channels which are not discovered by the optimisation process. The comparison of the saturation fields shows that there is less information in the observation data from certain

parts of the field in Example 5, than what is the case for Example 4. Due to this observation, it is natural that the field in Example 5 is the most difficult one to recover, and especially the regions with low flow may be problematic to reproduce.

From the comparison of the pressure data, it is more difficult to conclude anything about the amount of useful information in the data. It though seems like a constant gradient of the pressure field is preferable.

Returning to the convergence plots in Figure 17, we observe that the errors in the recovered  $c_j$ -values (Fig. 17 b)) are rather small for this example. Normally large errors in the contours will also force large errors in the  $c_j$ -values (see Ex. 2). This is not the case for this example. The low errors of the recovered  $c_j$ -values supports the conclusions from the analysis of the saturation fields, that the misclassified regions have small impact on the behaviour of the flow in the reservoir, and will thereby give a low response in the data.

As stated in Section 2, we have for simplicity neglected the capillary pressure ( $P_c = 0$ ) in our model. In a real case,  $P_c$  will be a nonzero continuous function depending on both the saturation and the spatial position  $\mathbf{x}$ . That is, over a discontinuity in the permeability field, there should be continuity in  $P_c$ , see [30]. It is reasonable to believe that a model with  $P_c \neq 0$  may give more information about the jumps in the permeability, than our simplified model will do. In this way, a recovery of the studied fields may be easier without our simplifications related to the capillary pressure functions. Studies of the history matching problem with  $P_c \neq 0$  is not looked into in this paper, but could be an issue for future works.

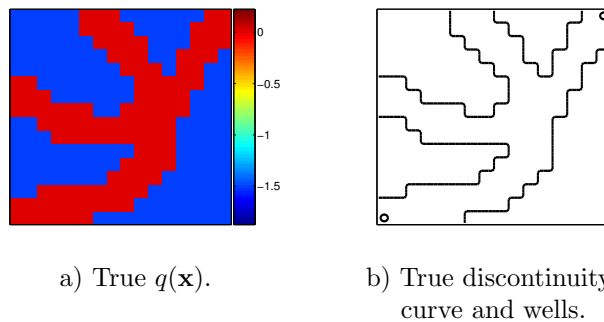


Figure 15: Example 5: True permeability and the corresponding discontinuity. The constant levels are given by  $\mathbf{c} = (-1.5, 0)$ , which corresponds to a permeability equal to 32 mD and 1 D. The circles in the corners are indicating the positioning of the wells.

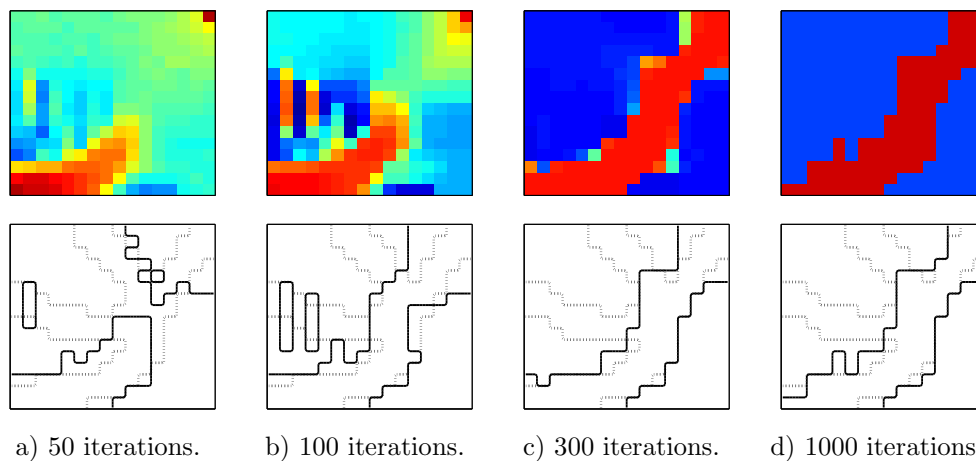


Figure 16: Example 5: The estimated permeability for different iterations. In the upper figures  $q^k$  is plotted with the same colourmap as used in Figure 15a). In the lower figures the signchanges of  $\phi^k$  are shown by the solid lines, and the discontinuities of the true  $q(\mathbf{x})$  are given by the dotted line. Only the parts of the channels in the main flow direction is recovered.

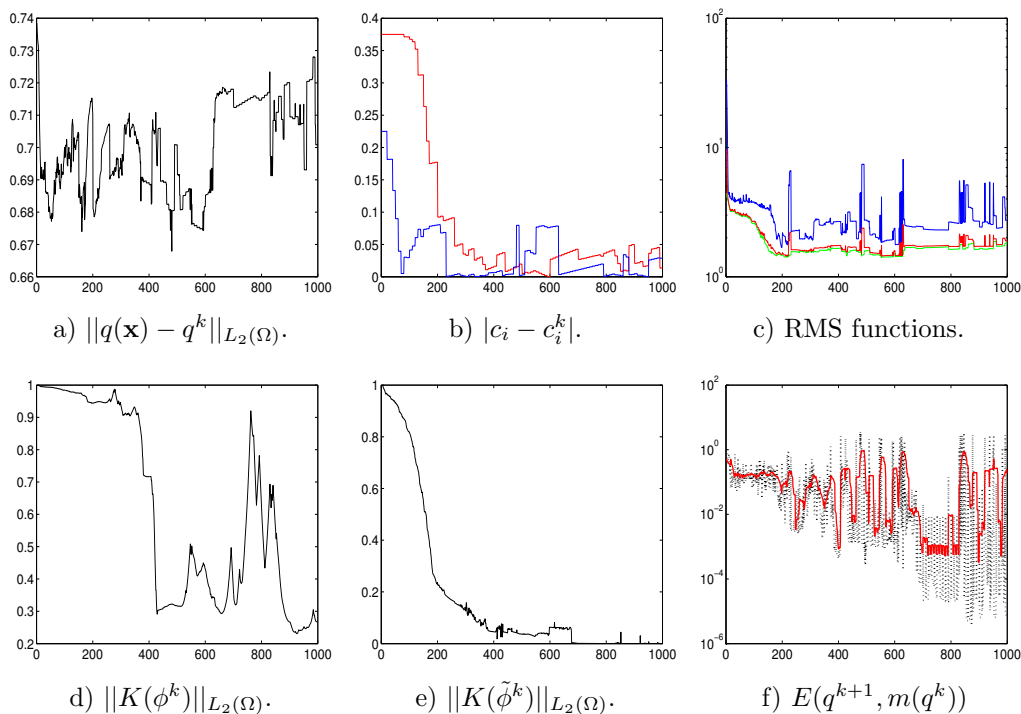


Figure 17: Example 5. Error measures and convergence plots versus the iteration number. Figure a) and b) give the error in the computed  $q^k$  and  $c_j^k$ -values. In Figure c) the red curve gives the RMS values of  $J_{tot}$ , while the blue and the green curves are the RMS functions for  $J_{well}$  and  $J_{seis}$ , respectively. Measures of the convergence of  $\phi^k$  and  $\tilde{\phi}^k$  are shown in Figure d) and e), respectively, while  $E(q^{k+1}, m(q^k))$  in Figure f) is the norm of the equation residual. The red curve in Figure f) is an average of  $E(q^{k+1}, m(q^k))$  for the last 15 iterations.

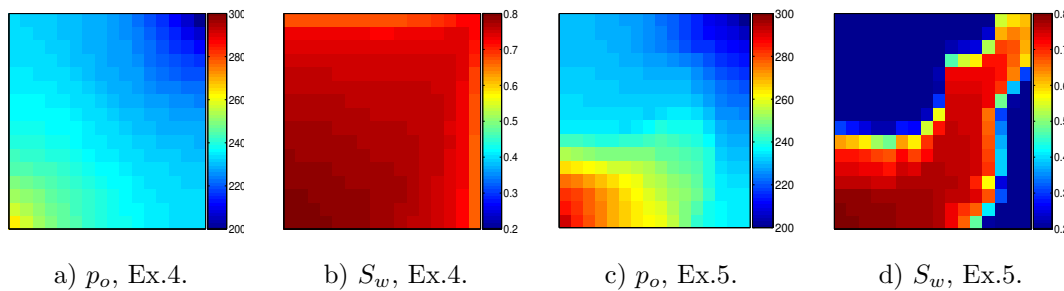


Figure 18: Comparison of seismic data of the true field. Pressure and saturation are plotted at end of simulation (3000 days). In Example 4,  $\mathbf{c} = (0, 0.3)$  and the injection rate is equal to 8% of the total pore volume per year, while in Example 5,  $\mathbf{c} = (-1.5, 0)$  and the injection rate is equal to 3.5% of the total pore volume per year. In Example 4 the complete field is flooded by water at the end of the simulation, while in Example 5 only parts of it is flooded.

## 9 Conclusions

We have applied a binary level set formulation for solving inverse two phase porous media flow problems. Both well data and seismic time-lapse data are utilised in the optimisation process.

The method is searching a piecewise constant solution of the inverse problem, and it is regularised by a total variation norm. By the proposed approach we can produce a solution with a predefined number of constant levels, and the geometries of the discontinuity curves are allowed to have arbitrary shapes only controlled by the total variation regularisation. To produce the results we do not need any initial guess of the geometries of discontinuities, only a reasonable guess of the constant levels is required.

The numerical studies focus on piecewise constant permeability fields with two different constant levels. On most of the tested examples the method is able to recover the main structures of permeability fields with rather complicated geometries and with a moderate amount of noise added to the observation data. Misclassifications of regions seem to be due to less information from the data in certain parts of the domain.

## 10 Acknowledgements

We gratefully acknowledge Daniel Christopher Doublet and Raymond Martinsen for providing their code for the forward reservoir simulator including gradient calculations, and for their help related to running this.

## References

- [1] O. Gosselin, S. van den Berg, and A Cominelli. Integrated history-matching of production and 4d seismic data. New Orleans, Louisiana, 30 Sept.-3 Oct. 2001. SPE 71599, Presented at the 2001 SPE Annual Technical Conference and Exhibition.
- [2] S.I. Aanonsen, A Cominelli, O Gosselin, I Aavatsmark, and T Barkve. Integration of 4D data in the history match loop by investigating scale dependent correlations in the acoustic impedance cube. 3-6 Sept. 2002. Proc. 8th European Conference on the Mathematics of Oil Recovery, Freiberg, Germany.
- [3] S.I. Aanonsen, I Aavatsmark, T Barkve, A Cominelli, R Gonard, O Gosselin, M Kolasinski, and H Reme. Effect of scale dependent data correlations in an integrated history matching loop combining production data and 4d seismic data. Feb. 2003. paper SPE 79665, presented at the SPE Reservoir Simulation Symposium held in Houston, Texas.

- 
- [4] G. Chavent and J. Liu. Multiscale parameterization for the estimation of a diffusion coefficient in elliptic and parabolic problems. In *Fifth IFAC Symposium on Control of Distributed Parameter Systems*, Perpignian, France, June 1987.
- [5] A. Trantola. *Inverse Problem Theory and Methods for Model Parameter Estimation*. SIAM, 2005.
- [6] A.J.W. Duijndam. Bayesian estimation in seismic inversion. Part I: Principles. *Geophysical Prospecting*, 36:878–898, 1998.
- [7] A.-A. Grimstad, T. Mannseth, G. Nævdal, and H. Urkedal. Adaptive multiscale permeability estimation. *Computational Geosciences*, 7(1):1–25, 2003.
- [8] I. Berre, M. Lien, and T. Mannseth. A level set corrector to an adaptive multiscale permeability prediction. Submitted 2004.
- [9] I. Berre, M. Lien, and T. Mannseth. Combined adaptive multiscale and level set parameter estimation. Submitted 2004.
- [10] S. Osher and J.A. Sethian. Fronts propagating with curvature-dependent speed: algorithms based on hamilton-jacobi formulations. *J. Comput. Phys*, 79(1):12–49, 1988.
- [11] X.-C. Tai and T. Chan. A survey on multiple level set methods with applications for identifying piecewise constant functions. *Int. J. of numerical analysis and modeling*, 1(1):25–47, 2004.
- [12] M. Burger. A level set method for inverse problems. *Inverse problems*, 17:1327–1355, 2001.
- [13] T. Chan and X.-C. Tai. Level set and total variation regularization for elliptic inverse problems with discontinuous coefficients. *Journal of Computational Physics*, 193:40–66, 2003.
- [14] E. Chung, Chan T., and X.-C. Tai. Electrical impedance tomography using level set representation and total variational regularization. submitted, 2004.
- [15] K. Ito, K. Kunisch, and Z. Li. Level-set function approach to an inverse interface problem. *Inverse problems*, 17:1225–1242, 2001.
- [16] O. Dorn, E. Miller, and C. Rappaport. A shape reconstruction method for electromagnetic tomography using adjoint fields and level sets. *Inverse Problems*, 16:1119–1156, 2000. Special issue on Electromagnetic Imaging and Inversion of the Earth’s Subsurface.
- [17] F. Santosa. A level-set approach for inverse problems involving obstacles. *ESAIM: Contr. Optim. Calc. Var.*, 1:17–33, 1996.
- [18] U. Ascher and E. Haber. Grid refinement and scaling for distributed parameter estimation problems. *Inverse Problems*, 17:571–590, 2001.
- [19] U. Ascher and E. Haber. Computational methods for large distributed parameter estimation problems with possible discontinuities. *Symp. Inverse Problems, Design and Optimization*, 2004.
- [20] U. Ascher, E. Haber, and H. Huang. On effective methods for implicit piecewise smooth surface recovery. Submitted 2004.
- [21] M. Burger and S. Osher. A survey on level set methods for inverse problems and optimal design. UCLA, Applied Mathematics, CAM-Report 04-02, 2004.
- [22] J. Lie, M. Lysaker, and X.-C. Tai. A piecewise constant level set framework. url:”<http://www.mi.uib.no/BBG/papers.html>”, 2004.
- [23] J. Lie, M. Lysaker, and X.-C. Tai. A piecewise constant level set level set framework. In *European Congress on Computational Methods in Applied Sciences and Engineering*, Jyväskylä, July 2004.

- 
- [24] J. Lie, M. Lysaker, and X.-C. Tai. A binary level set model and some applications to mumsford-shah image segmentation. Accepted and to appear in IEEE Transaction on image processing, 2005.
- [25] L. K. Nielsen, X.-C. Tai, S.I. Aanonsen, and M Espedal. A binary level set model for elliptic inverse problems with discontinuous coefficients. UCLA, CAM-report, 2005.
- [26] X.-C. Tai, O. Christiansen, P. Lin, and I. Skjaelaaen. A remark on the mbo scheme and some piecewise constant level set methods. UCLA, Applied Mathematics, CAM-report-05-24, 2005.
- [27] F. Gibou and R. Fedkiw. Fast hybrid k-means level set algorithm for segmentation. *Stanford Technical Report*, November 2002.
- [28] B. Song and T. Chan. A fast algorithm for level set based optimization. *UCLA CAM-report-68*, 2002.
- [29] R. Li, A.C. Reynolds, and D.S. Oliver. History matching of three-phase flow production data. *SPE Journal*, 8(4), December 2003.
- [30] B.G. Ersland, M. Espedal, and R. Nybø. Numerical methods for flow in a porous medium with internal boundaries. *Computational Geosciences*, 2:217–240, 1998.